

## Article

# Comparison of Phase-Locked Loops Used for Frequency Measurements in a Low-Inertia Power Grid with Wind Generation

Orlando David Guerrero-Bermúdez <sup>1</sup>, Sergio Martinez <sup>1,\*</sup>, Eder Molina <sup>2</sup> and John E. Candelo-Becerra <sup>3</sup><sup>1</sup> Escuela Técnica Superior de Ingenieros Industriales, Universidad Politécnica de Madrid, 28040 Madrid, Spain<sup>2</sup> Centro de Investigación Audacia, Universidad Simón Bolívar, Barranquilla 080002, Colombia<sup>3</sup> Facultad de Minas, Departamento de Energía Eléctrica y Automática, Universidad Nacional de Colombia-Sede Medellín, Carrera 80 No. 65-223, Robledo, Medellín 050041, Colombia

\* Correspondence: sergio.martinez@upm.es

**Abstract:** The need for more precise frequency measurements in electric power systems is increasing because of the growing penetration of renewable energy and the subsequent reduction in inertia, which gives rise to more intense frequency fluctuations. Phase-locked loops (PLLs) are now more accurate and present faster dynamic responses, helping to implement primary frequency controllers for renewable generators connected to the grid through power electronics. However, there are differences among PLL implementations that affect their behavior when estimating frequency, depending on factors as location, voltage level, or penetration of renewable energy, among other things. How this affects the ability of PLL-based frequency controllers to adequately estimate the instantaneous mismatch between generation and demand, especially in low-inertia power systems, is still unclear, and constitutes an open research topic. This paper contributes to this research effort by presenting a comparative study of different PLL configurations in order to gain insight into their performance in different scenarios in a low-inertia power system with a high share of wind energy. Constant and variable wind speed scenarios are considered, and PLL behavior is assessed in terms of the absolute mean value and the root-mean-square value of the frequency error, and the absolute value of the frequency derivative error. The results show that the PLL behavior depends on the voltage level and the location, and it was found that the further away the PLL is from the source that controls the frequency, the more noise is produced, which impacts the quality of the frequency measurement.

**Keywords:** frequency; wind generator; synchronous machine; phase-locked loop; low-inertia power grid



**Citation:** Guerrero-Bermúdez, O.D.; Martinez, S.; Molina, E.; Candelo-Becerra, J.E. Comparison of Phase-Locked Loops Used for Frequency Measurements in a Low-Inertia Power Grid with Wind Generation. *Electronics* **2022**, *11*, 3226. <https://doi.org/10.3390/electronics11193226>

Academic Editors: Shailendra Rajput, Moshe Averbukh and Noel Rodriguez

Received: 31 August 2022

Accepted: 6 October 2022

Published: 8 October 2022

**Publisher's Note:** MDPI stays neutral with regard to jurisdictional claims in published maps and institutional affiliations.



**Copyright:** © 2022 by the authors. Licensee MDPI, Basel, Switzerland. This article is an open access article distributed under the terms and conditions of the Creative Commons Attribution (CC BY) license (<https://creativecommons.org/licenses/by/4.0/>).

## 1. Introduction

The current trend in electric power systems of displacing conventional power plants by renewable energy ones has unquestionable environmental and economic benefits, but it also poses new challenges. Apart from the evident intermittent character of renewable resources, photovoltaic solar and wind energies also cause some stability, power quality, and reliability issues [1,2]. In contrast to conventional synchronous generators, which are directly connected to the grid, renewable generators are mainly connected through electronic converters [3]. This decoupling reduces the synchronous equivalent inertia of the power system [4] and impacts its dynamic behavior in the case of disturbances of different natures [5].

In alternating current power systems, the rotational speed of online synchronous generators determines the frequency of current and voltage waveforms. Under steady-state conditions, all synchronous generators in the power system rotate at the same electrical speed, which is proportional to the unique system frequency. The frequency deviation from its rated value (50 or 60 Hz) is closely related to the transient differences between the mechanical power input to synchronous generators and the electrical power demand. These mismatches are assumed by the kinetic energy stored in rotating masses, impacting the

rotational speed of the generators and, consequently, the system's frequency. This natural inertial response of conventional generators to mismatches in the demand–generation balance is not present in renewable generators connected to the grid through electronic converters. To include the power response of these generators to frequency variations, their controllers must include accurate frequency measurements at the connection point.

A phase-locked loop (PLL) is the most common technology for performing frequency measurements in a power system, helping to synchronize the power converters with the grid. In addition, it is now widely used because its indirect measurement system detects deviations quickly, contributing to the frequency, voltage, and power control of the network, which are required to maintain power system stability.

There are various PLL technologies applied in power converters, some of them used for different applications and studies, including the synchronous reference frame PLL (SRF-PLL) [6], Lag PLL (LAG-PLL) [7], Low-Pass Filter PLL (LPF-PLL) [8], Enhanced PLL (E-PLL) [9], Moving Average Filter PLL (MAF-PLL) [10], second-order generalized integrator–frequency-locked loop (SOGI-FLL) [11], second-order generalized integrator PLL (SOGI-PLL) [12], and double second-order generalized integrator PLL (DSOGI-PLL) [13]. As the commercial PLLs consider a wide variety of devices that comply with the measurement function using different methods, it is interesting to evaluate the behavior of each one under different signal variations, for example, due to wind speed variations.

Some authors have compared the use of PLLs for power system applications. For example, the authors of [14] performed experimental tests of PLLs implemented on a digital signal processor (DSP), comparing the filtering capacities of SRF-PLL, E-PLL, QPLL, and DSOGI-PLL. They considered internal and external filtering harmonics in the voltage to identify the behaviors and solutions provided by each PLL implementation. However, other PLLs were not included, and the frequency response on different locations in a power system was not considered. In [15], the authors performed simulations and experiments to compare SRF-PLL algorithms under distorted utility conditions to perform a performance evaluation. However, not all PLLs were evaluated in this research.

In [8], the authors evaluated different PLLs to develop improved noise filtering and reduce numerical spikes after sudden variations of the voltage at the AC bus of the converter. The paper compared the dynamic behavior of SRF-PLL, Lag-PLL, LPF-PLL, E-PLL, and SOGI-FLL, considering both contingencies and noise [8]. However, these PLLs were not tested to evaluate the frequency behavior in different buses and consider wind speed variations. In [16], the authors compared SRF-PLL, LAG-PLL, LPF-PLL, E-PLL, and SOGI-FLL to estimate frequency deviations. They used the IEEE nine-bus test power system, and the evaluation focuses on accuracy and sensitivity to noise. However, they evaluated the system at one bus, and no wind speed scenarios were considered. In [17], a comparison of the performance of SRF-PLL, DSRF-PLL, and DSOGI-PLL was presented in response to the grid voltage magnitude changes with symmetrical and asymmetrical changes similar to those found in rural networks with renewable energies. In this last paper, the authors used a general power system model and focused on balanced and unbalanced grid voltage scenarios. In [18], a comparison of the SOGI-FLL and the SOGI-PLL for single-phase grid-connected inverters was presented. The authors considered frequency and voltage magnitude changes of a single-phase power input.

In [19], the authors conducted a comparison of SRF-PLL, DSOGI-PLL, enhanced synchronous reference frame PLL (ESRF-PLL), and Decoupled Double Synchronous Reference Frame PLL (DDSRF-PLL) to estimate the system frequency under unbalances, harmonics, and frequency variations. However, they evaluated the performance of PLLs in a numerical case study and did not consider a system with renewable energy sources. In [20], the authors compared the PLL and SRF controllers for six-pulse D-STATCOM to compensate voltage flicker due to electric arc furnace load in the IEEE 13 distribution bus test system. They only considered the main energy source and a medium-sized industrial plant, and did not compare other PLLs. In [21], the authors validated the performance of different PLLs under voltage-sag, varying grid frequency, phase jump, and dc-offset disturbances on

the basis of simulation and experimental results. They modeled the SOGI-PLL, cascaded SOGI-PLL (CSOGI-PLL), second-order SOGI-PLL (SO-SOGI-PLL), modified SOGI-PLL (MSOGI-PLL), and mixed second- and third-order generalized integrator PLL (MSTOGI-PLL). They performed simulation and experimental tests to evaluate power quality by changing the parameters of the source and without considering other types of sources.

In [22], the authors evaluated the SRF-PLL, MAF-PLL, and cascaded delayed signal cancellation PLL (CDSC-PLL) for grid voltages contaminated with interharmonics in the presence of different grid disturbances, such as frequency jump, phase angle jump, and dc offset. They performed the test by changing the grid parameters to evaluate the performance of the PLLs, but they did not use a power system with different voltages and renewable sources. In [23], the authors compared the behavior of abc reference frame PLL (abc-PLL), stationary reference frame PLL ( $\alpha\beta$ -PLL), synchronous reference frame PLL (dq-PLL), voltage reforming synchronous reference frame PLL (VRSR-PLL), and decoupled double synchronous reference frame PLL (DDSRF-LL) under balanced and unbalanced voltages. They changed the grid voltage parameters to perform the test, and no detailed power system models were included to represent wind energies.

To the best of our knowledge, the literature review shows that PLLs are widely used, and have been compared for different applications in order to evaluate their measurement capacities. However, some authors compare few PLLs [17], do not perform an evaluation on different voltage levels in the power network [18], or do not consider wind speed scenarios [8]. In addition, other papers have compared PLLs in other applications [22,24–26]. In summary, there are differences among PLL implementations that affect their behavior when estimating frequency, depending on factors such as location, voltage level or penetration of renewable energy, among others. How this affects the ability of PLL-based frequency controllers to adequately estimate the instantaneous mismatch between generation and demand, especially in low-inertia power systems, is still unclear and constitutes an open research topic.

The aim of the work presented in this paper is to contribute towards this research effort by presenting a comparative study of different PLL configurations to gain insight on their performance in different scenarios of a low-inertia power system with high share of wind energy. This study is conducted on the basis of simulations on a test power system with a synchronous generator, a wind farm, and a constant impedance load, and it is structured as follows: (1) Different PLLs (SRF-PLL, LAG-PLL, SOGI-PLL, DSOGI-PLL, and MAF-PLL) are located at different buses in the power system and their performance on dynamic frequency measurement is compared. (2) The simulations are carried out in two operation scenarios for the wind generators: with constant wind speed (steady-state operation) and with variable wind speed (small signal disturbances). (3) The work analyzes the measurement error of the PLLs with typical deviation indexes compared to the rotation speed of the synchronous generator, used as reference. (4) The research concludes by identifying the configurations that best suit the needs at different operation points of the power system.

In summary, constant and variable wind speed scenarios are considered, and the PLL behavior is assessed in terms of the absolute mean value and the root-mean-square value of the frequency error, and the absolute value of the frequency derivative error. The results show that the PLL behavior depends on the voltage level and the location, indicating that the further away the PLL is from the source that controls the frequency, the more noise is produced, which impacts the quality of the frequency measurement.

The remainder of the paper is structured as three more sections. Section 2 outlines the materials and methods, where the general concepts, diagrams, and mathematical models of the PLLs are presented. In addition, this section includes the power system models and parameters and defines the scenarios chosen to perform the tests. Section 3 presents the frequency measurement results and the errors from each PLL implementation at different buses in the test power system, including a summary of the advantages and drawbacks

of the different alternatives. Finally, Section 4 summarizes the conclusions and suggests future work.

## 2. Materials and Methods

This section introduces the theoretical foundation of PLLs, the general description of each PLL, the scenarios used to perform the comparison, and the power system used to evaluate the methods.

### 2.1. Phase-Locked Loop

A PLL is a power electronic application that indirectly measures frequency, voltage magnitude, and voltage angle. These variables are essential to identifying the operating state of a power system. All signals are monitored to guarantee the power system stability according to the applicable standards.

Figure 1 presents a basic diagram of a PLL, comprising a phase detector (PD), a loop filter (LF), and a voltage-controlled oscillator (VCO).

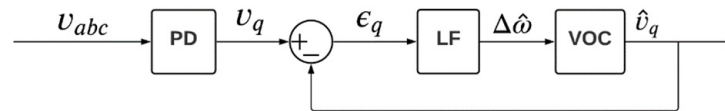


Figure 1. Basic diagram of a phase-locked loop (PLL).

The PLL works by receiving a single-phase or three-phase voltage signal and returning signals through algorithms with fast and precise detection, such as the network frequency.

#### 2.1.1. Phase Detector (PD)

The PD uses a three-phase voltage vector at the desired measurement point,  $v_{abc}(t)$ , as shown in Figure 2a. This voltage is converted using spatial vectors from an  $abc$  representation (see Figure 2a) to an  $\alpha\beta$  representation (see Figure 2b).

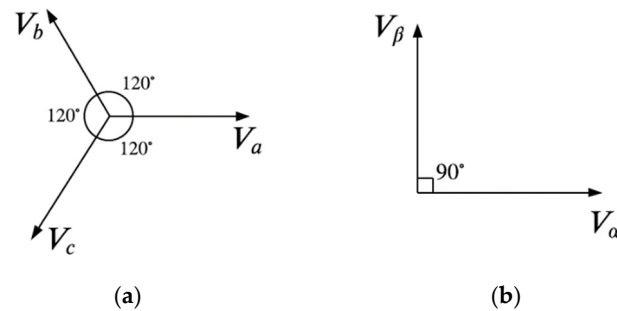


Figure 2. Clarke transformation [27]: (a)  $abc$  representation and (b)  $\alpha\beta$  representation.

The three-phase voltages of a balanced network are given by Equation (1):

$$V_{abc} = \begin{bmatrix} v_a \\ v_b \\ v_c \end{bmatrix} = V_m \begin{bmatrix} \cos(\omega t + \theta_a) \\ \cos(\omega t + \theta_a - 2\pi/3) \\ \cos(\omega t + \theta_a + 2\pi/3) \end{bmatrix}, \tag{1}$$

where  $v_a$ ,  $v_b$ , and  $v_c$ , are the instantaneous phase voltages,  $V_m$  is the voltage amplitude,  $\theta_a$  is the  $v_a$  initial phase angle, and  $\omega$  is the angular frequency.

The Clarke transformation is given by Equation (2):

$$\begin{bmatrix} V_\alpha \\ V_\beta \end{bmatrix} = \frac{2}{3} \begin{bmatrix} 1 & -1/2 & -1/2 \\ 0 & \sqrt{3}/2 & -\sqrt{3}/2 \end{bmatrix} \begin{bmatrix} v_a \\ v_b \\ v_c \end{bmatrix}. \tag{2}$$

This can be written in a more compact way as Equation (3):

$$V_{\alpha\beta} = [T_{\alpha\beta}] V_{abc}. \quad (3)$$

The  $\alpha\beta$  representation can be simplified as shown in Equation (4), where  $\theta$  is the instantaneous angle of the angular frequency  $\omega$  ( $\theta = \omega t + \theta_0$ ):

$$\begin{bmatrix} V_\alpha \\ V_\beta \end{bmatrix} = V_m \begin{bmatrix} \cos \theta \\ \sin \theta \end{bmatrix}. \quad (4)$$

The phase angle  $\theta$  can be tracked by synchronizing the voltage vector along the direct axis ( $d$ ). The  $\alpha\beta$  stationary reference frame is transformed into a rotating reference frame ( $dq$ ) using the Park transform, as shown in Figure 3.

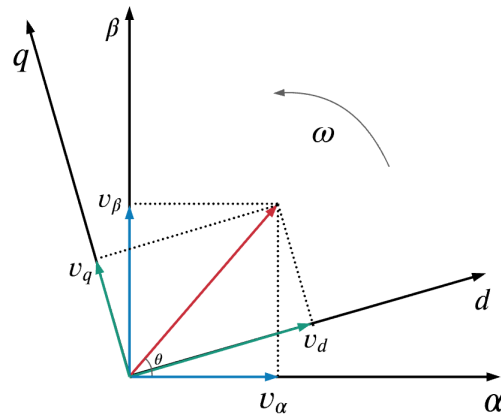


Figure 3. Park and Clarke transformations [28].

Equation (5) presents the Park transform, where  $\theta'$  is the instantaneous angle of the rotating reference frame. Equation (5) can be written in a more compact way as Equation (6).

$$\begin{bmatrix} V_d \\ V_q \end{bmatrix} = \begin{bmatrix} \cos(\theta') & \sin(\theta') \\ -\sin(\theta') & \cos(\theta') \end{bmatrix} \begin{bmatrix} V_\alpha \\ V_\beta \end{bmatrix} \quad (5)$$

$$V_{dq} = [T_{dq}] V_{\alpha\beta} \quad (6)$$

Equation (7) displays the  $dq$  transform, as a combination of Park and Clarke transformations.

$$\begin{bmatrix} V_d \\ V_q \end{bmatrix} = [T_{dq}] [T_{\alpha\beta}] V_{abc} = V_m \begin{bmatrix} \cos(\theta - \theta') \\ \sin(\theta - \theta') \end{bmatrix}. \quad (7)$$

### 2.1.2. Loop Filter (LF)

After transforming the voltage signal from  $abc$  to  $dq$ , the loop filter (LF) compares the error  $\varepsilon_q(t)$  between the voltage measurement on the  $q$  axis and the value estimated by the PLL. Several methods are used in PLLs to perform filtering, including stages such as attenuation, low-pass filtering, or high-pass filtering.

### 2.1.3. Voltage-Controlled Oscillator (VCO)

After the signal is filtered, it enters the voltage-controlled oscillator (VCO), which takes the frequency deviation and provides the estimation of the  $q$ -axis component to obtain the error  $\varepsilon_q(t)$ . The VCO generally consists of a pure integrator to avoid steady-state signal noise.

### 2.2. Phase-Locked Loop Configurations

Different PLLs on the market can measure frequency. Some of these configurations are reviewed to identify their characteristics and compare their functioning.

#### 2.2.1. Synchronous Reference Frame PLL (SRF-PLL)

Synchronous reference frame PLL (SRF-PLL) is one of the most used types today, and is one of the simplest to implement. This PLL considers a PD modeled as a pure delay, the LF is implemented with a PI controller, and the VCO is an integrator [14,29], as displayed in Figure 4.

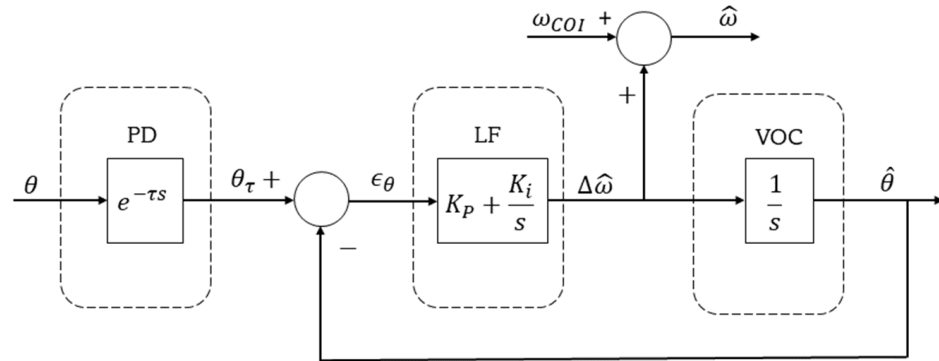


Figure 4. Diagram of the synchronous reference frame (SRF)-PLL.

#### 2.2.2. Lag-PLL

Lag-PLL is an SRF-PLL with a low-pass filter before the PI on the LF, as indicated in Figure 5. A low-pass filter after the  $T_{dq}$  transform reduces the sensitivity of the PLL to harmonics (or noise), preventing numerical errors in the frequency measurement [15].

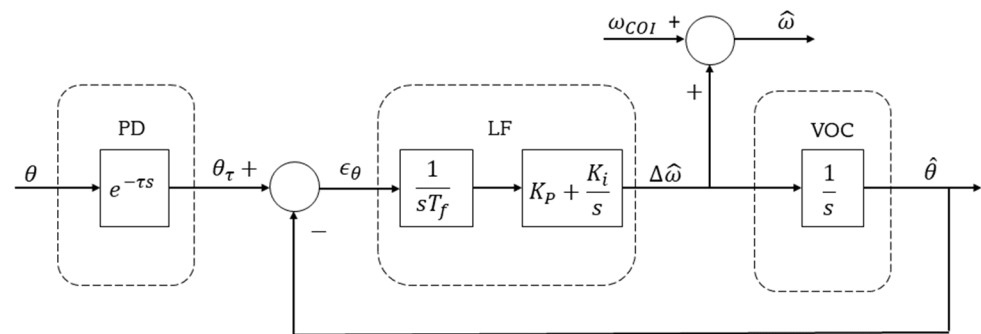


Figure 5. Diagram of the Lag-PLL.

#### 2.2.3. Second-Order Generalized Integrator PLL (SOGI PLL)

This PLL is typically used in single-phase systems and works under the concept of the second-order generalized integrator (SOGI) for sinusoidal signals [30], as presented in Figure 6. As stated in [31], this integrator is derived from the principle whereby the time domain convolution product of a sinusoidal function gives the original function multiplied by the time variable. Therefore, a processing block, whose transfer function matches the Laplace transform of a sinusoidal function, will act as an amplitude integrator for a sinusoidal signal applied to its input. Furthermore, the quadrature combination of the sine and cosine transfer functions gives rise to an ideal integrator independent of the phase angle of the sinusoidal input signal.

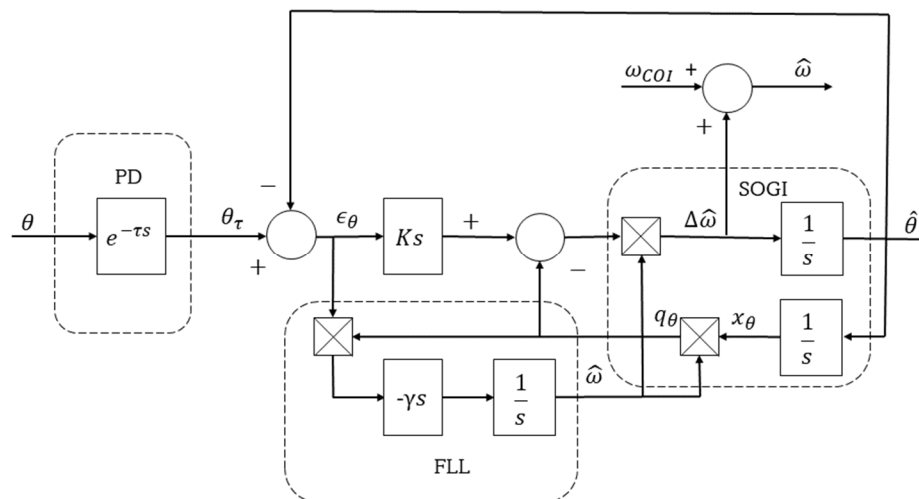


Figure 6. Diagram of the SOGI-PLL.

Figure 7 presents the low-pass filter stage of the SOGI-PLL.

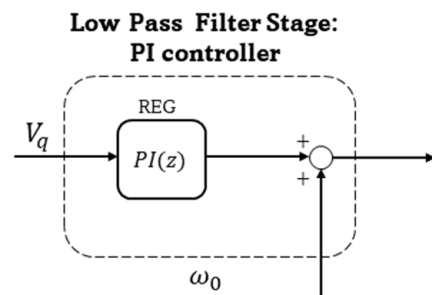


Figure 7. Low-pass filter of the SOGI-PLL.

#### 2.2.4. Dual Second-Order Generalized Integrator PLL (DSOGI-PLL)

For three-phase systems, it is common to use two SOGIs in parallel, as specified in Figure 8. The signal then enters an SRF-PLL to take advantage of its filtering characteristics. This provides excellent protection against voltage unbalances in the network. This technique has demonstrated fast, accurate, and adaptive frequency response to grid fault conditions [32].

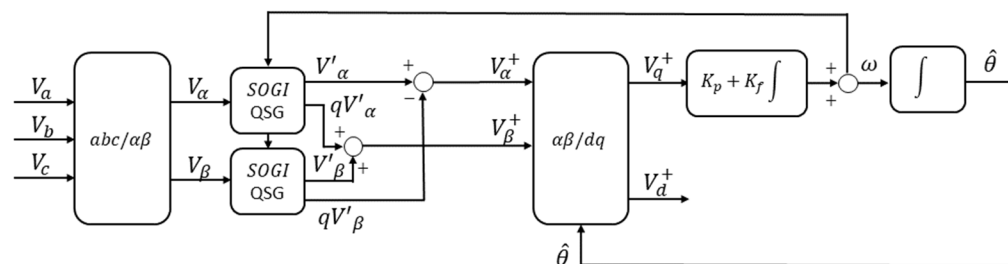


Figure 8. Diagram of the DSOGI-PLL.

#### 2.2.5. Moving Average Filter PLL (MAF-PLL)

This configuration, presented in Figure 9, is like the Lag-PLL, which adds a filter before the PI (MAF) to reject harmonics in the frequency measurement. The representation of the signal  $x(t)$  is defined as follows [33]:

$$\bar{x}(t) = \frac{1}{T_\omega} \int_{t-T_\omega}^t x(\tau) d\tau. \tag{8}$$

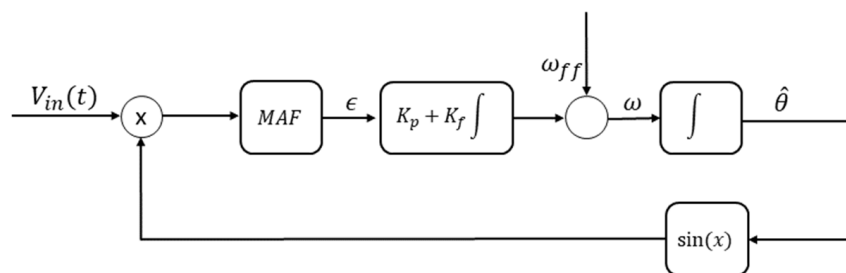


Figure 9. Diagram of the MAF-PLL.

Finally, Figure 10 shows the MAF-PLL configuration, which considers the transformation from  $\Delta\omega$  to frequency (Hz).

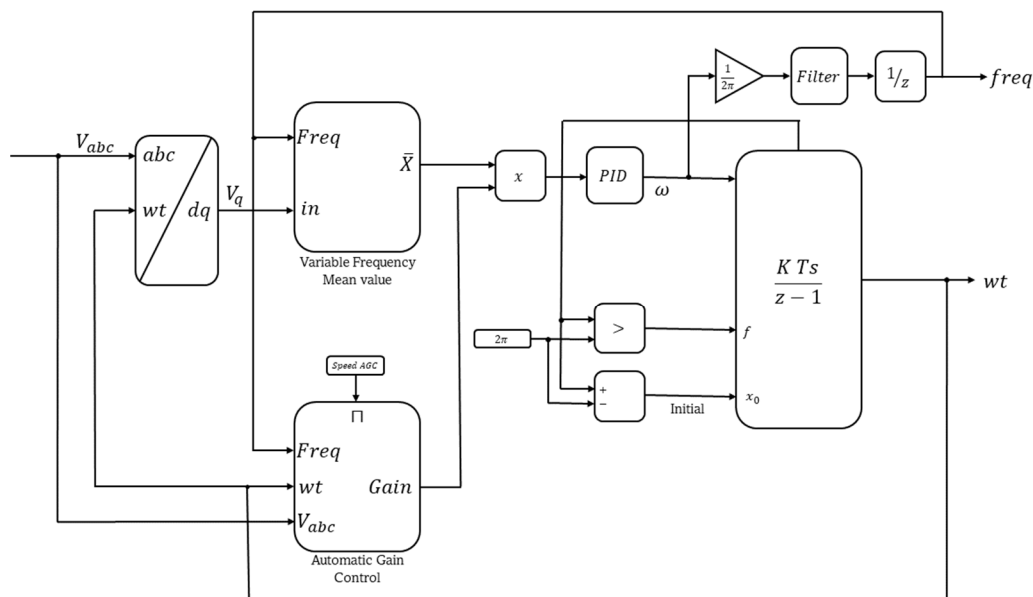
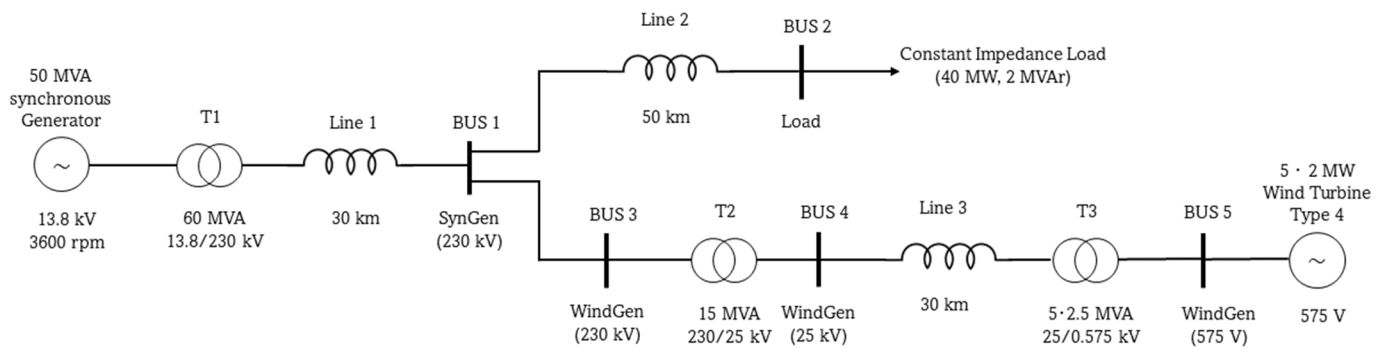


Figure 10. Diagram of the MAF-PLL VCO (voltage-controlled oscillator).

### 2.3. Test Power System

Figure 11 shows the power system test case used to compare the PLLs. This system considers a 50 MVA synchronous machine, a 10 MVA wind farm, and a three-phase parallel load with 40 MW and 2 MVar (constant impedance load). The system inertia is provided by a steam turbine with a synchronous machine of 13.8 kV, and 3600 rpm. This turbine is controlled by a primary steam engine composed in complete tandem, including a speed control system, turbine steam with four stages, and a simple mass axis. The time constants and regulation parameters are obtained by considering the elements used in the research [34,35] and summarized in Table 1. A power system stabilizer (PSS) provides frequency and voltage stability control, which adds damping to the oscillations of the synchronous machine rotor by controlling its excitation, thus maintaining the system stability [36].

Five wind turbines of 2 MW are represented in the power system, considering the model proposed in [37]. Each type 4 wind turbine consists of a synchronous generator connected to a rectifier, a PWM boost converter based on a DC/DC IGBT, and a PWM converter based on a DC/AC IGBT with voltage sources. This type 4 technology achieves maximum wind energy for low wind speeds by optimizing turbine speed while minimizing mechanical stresses during wind gusts [37].



**Figure 11.** Power system test case used to compare the PLLs.

**Table 1.** Time constants and reactance parameters of the synchronous machine used in the study.

Parameter	Symbol	Value
$d$ -axis subtransient short-circuit time constant	$T_d''$	0.023 s
$d$ -axis transient short-circuit time constant	$T_d'$	1.32 s
$d$ -axis transient open-circuit time constant	$T_{do}'$	4.5 s
Armature time constant	$T_a$	0.15 s
Subtransient $d$ -axis reactance	$X_d''$	20%
Transient $d$ -axis reactance	$X_d'$	25%
$d$ -axis reactance	$X_d$	165%

Transmission lines are represented by a  $\pi$  model, following the recommendations of [38]. Two winding three-phase transformers are used to step up the voltage of the synchronous machine from 13.8 kV to 230 kV, and the wind turbine from 575 V to 25 kV and from 25 kV to 230 kV. The connections of the power transformers are carried out following the recommendations of [39].

#### 2.4. Case Study

The different PLL configurations were evaluated on the basis of simulations of the test power system with MATLAB/Simulink. Just as an example of the implementation of the models in Simulink, Figure 12 shows a screenshot of the Simulink model 7 of the wind turbine used.

Simulations consider two different wind scenarios in the test power system under study:

- Scenario 1: Frequency measurement with a constant wind speed (15 m/s), constant load, and reactive power reference at 0 var.
- Scenario 2: Frequency measurement with variable wind speed data taken from [40] (day 055 of 1992), as presented in Figure 13. The speed data are expressed in m/s, sampled at 25 Hz (samples every 40 ms). A period of 430 s is considered for this study, with the wind speed kept constant for the first 130 s.

The frequency was measured with the PLLs located at the following buses presented in Figure 11:

- (1) 230 kV bus in the synchronous generator zone (230 kV SynGen bus);
- (2) 230 kV bus in the load zone (230 kV Load bus);
- (3) 230 kV bus in the wind generator zone (230 kV WinGen bus);
- (4) 25 kV bus in the wind generator zone (25 kV WinGen bus); and
- (5) 575 V bus in the wind generator zone (575 V WinGen bus).

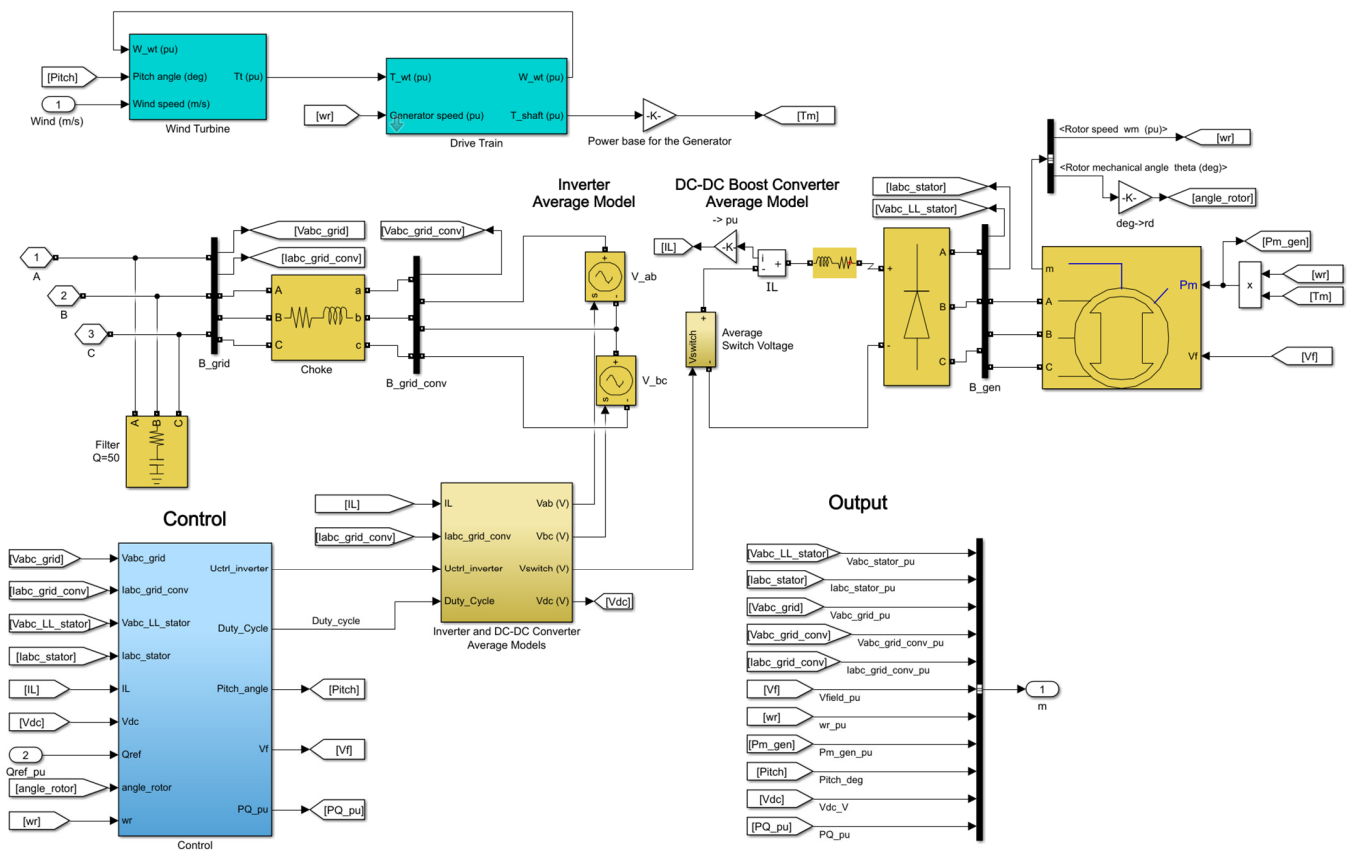


Figure 12. Simulink model of the wind generator and the control system.

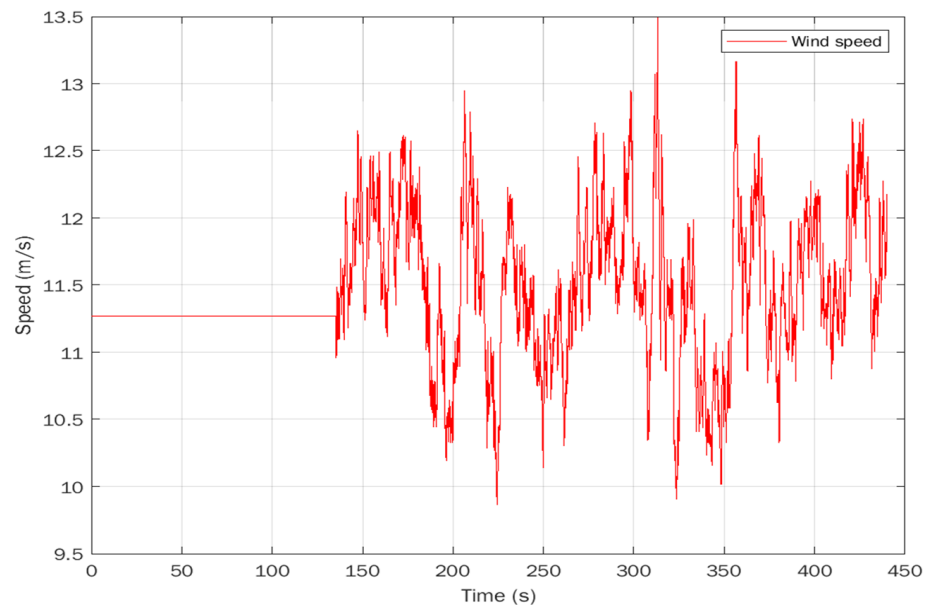


Figure 13. Variable wind speed data.

### 2.5. Measurement Deviation

The way to compare data is by calculating the measurement deviation. This value is compared to the reference speed of the synchronous machine. For this calculation, some comparison methodologies are used, related to indirect measurement, as described below.

### 2.5.1. Mean Absolute Error

The mean absolute error (MAE) is commonly used to compare predicted versus measured values. It can be used to compare different measurement techniques with an observable reference in several events. The mean absolute error (MAE) is the average value of the error  $e_i$  as presented in Equation (9), where  $n$  is the number of samples,  $y_i$  is the measured value, and  $x_i$  is the reference value [41].

$$MAE = \frac{\sum_{i=1}^n |e_i|}{n} = \frac{\sum_{i=1}^n |y_i - x_i|}{n}. \quad (9)$$

It can be expressed as a percentage of the reference values as:

$$MAE\% = \frac{\sum_{i=1}^n |y_i/x_i - 1|}{n} 100. \quad (10)$$

### 2.5.2. Root-Mean-Square Error

The root-mean-square error (RMSE) is a statistical metric commonly used for electrical magnitudes because of its usefulness in studying periodic waveforms. It gives the square root of the mean value of the squared function of the instantaneous deviations, as shown in Equation (11):

$$RMSE = \sqrt{\frac{\sum_{i=1}^n (y_i - x_i)^2}{n}}. \quad (11)$$

Or, as a percentage of the reference, as follows:

$$RMSE\% = \sqrt{\frac{\sum_{i=1}^n (y_i/x_i - 1)^2}{n}} 100. \quad (12)$$

### 2.5.3. Error of the Frequency Derivative

The analysis of the derivative of the frequency, also known as rate of change of frequency (RoCoF), is interesting for assessing the effectiveness of frequency control in power systems. For a given sample  $y_i$  at time  $t_i$ , it can be computed as in Equation (13):

$$RoCoF_i = \frac{y_i - y_{i-1}}{t_i - t_{i-1}}. \quad (13)$$

To assess the behavior of different PLLs in relation to their ability to track the RoCoF, in this work we use the absolute error of the frequency derivative (AEFD). For a given sample, it can be computed in terms of the reference signal  $x$  as:

$$AEFD_i = \left| RoCoF_i - \frac{x_i - x_{i-1}}{t_i - t_{i-1}} \right|. \quad (14)$$

As global metrics for a given period with  $n$  samples, in this work we use the cumulative relative AEFD (CAEFD%) and the cumulative relative root-mean-square error of the frequency derivative (CRMSEFD%), defined as:

$$CAEFD\% = \sum_{i=1}^n \left| \frac{RoCoF_i}{\frac{x_i - x_{i-1}}{t_i - t_{i-1}}} - 1 \right| 100. \quad (15)$$

$$CRMSEFD\% = \sqrt{\sum_{i=1}^n \left( \frac{RoCoF_i}{\frac{x_i - x_{i-1}}{t_i - t_{i-1}}} - 1 \right)^2} 100. \quad (16)$$

### 3. Results and Analysis

This section compares different PLLs in two scenarios (Scenario 1: constant wind speed and Scenario 2: variable wind speed). The error metrics (MAE%, RMSE% and AEFD%) are quantified and compared to identify the advantages and disadvantages of each PLL.

#### 3.1. Scenario 1: Constant Wind Speed

This scenario is characterized by a constant wind speed of 15 m/s in the wind farm and an almost constant load, only disturbed by 1% step variations every 10 s. Figure 14 shows the frequency measurements with the PLLs located at the 230 kV WinGen bus during quasi-steady-state operation of the power system. Figure 14a presents the system frequency measured with the PLLs from seconds 15 to 35. This figure illustrates that all PLLs measure the frequency similarly in the 230 kV network, with values close to the reference. This frequency reference is computed as the product of the per unit rotational speed of the synchronous generator and the rated frequency (60 Hz). There are slight differences in the PLLs that are not easily perceived in this first figure because of the scale.

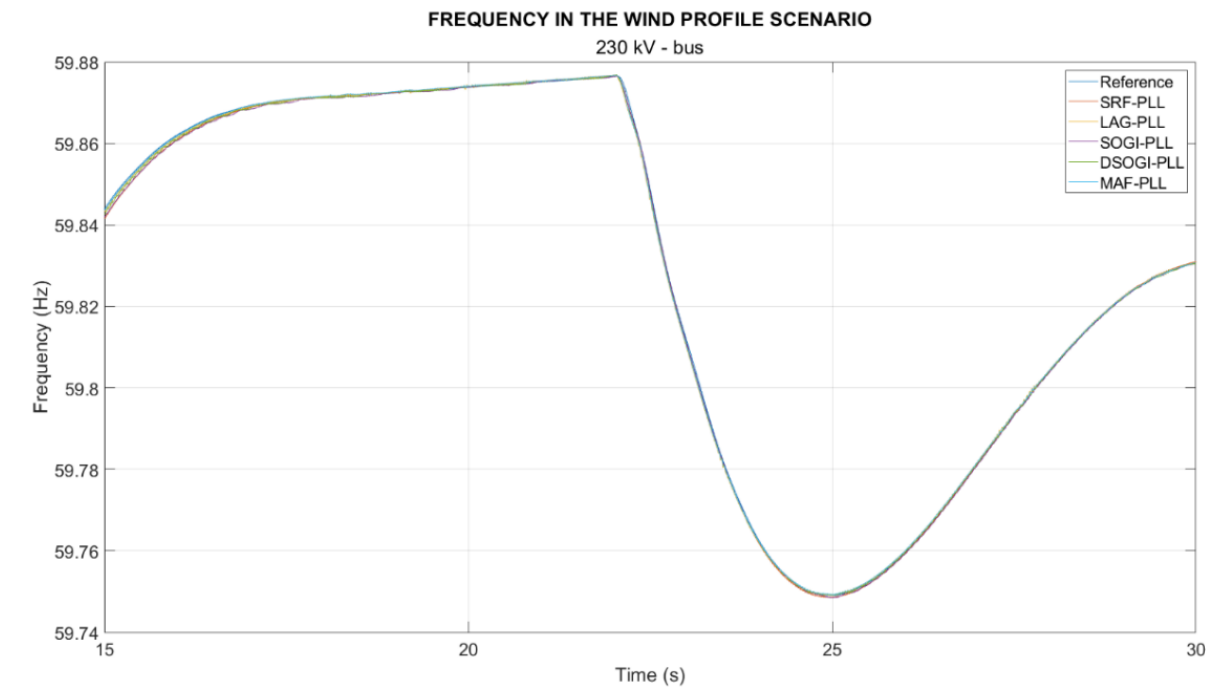
To better appreciate the differences, Figure 14b presents a zoomed-in image of the interval from seconds 22 to 22.2. As can be seen, different PLL implementations give rise to slight differences in comparison with the frequency reference, but most are close to representing the same behavior. In addition, the MAF averages the frequency signal more linearly than the other PLLs. The SRF-PLL, the simpler implementation, presents the most significant differences from the reference in the 230 kV network.

Figure 15 shows analogous frequency measurements but with the PLLs located at the 25 kV WinGen bus. Figure 15a presents the system frequency measured with the PLLs from seconds 15 to 35. As Figure 14a, it shows that all PLLs measured a frequency similar to that of the reference. However, compared to the slight differences presented in the 230 kV WinGen bus, the values obtained in the 25 kV WinGen bus present larger differences from the reference.

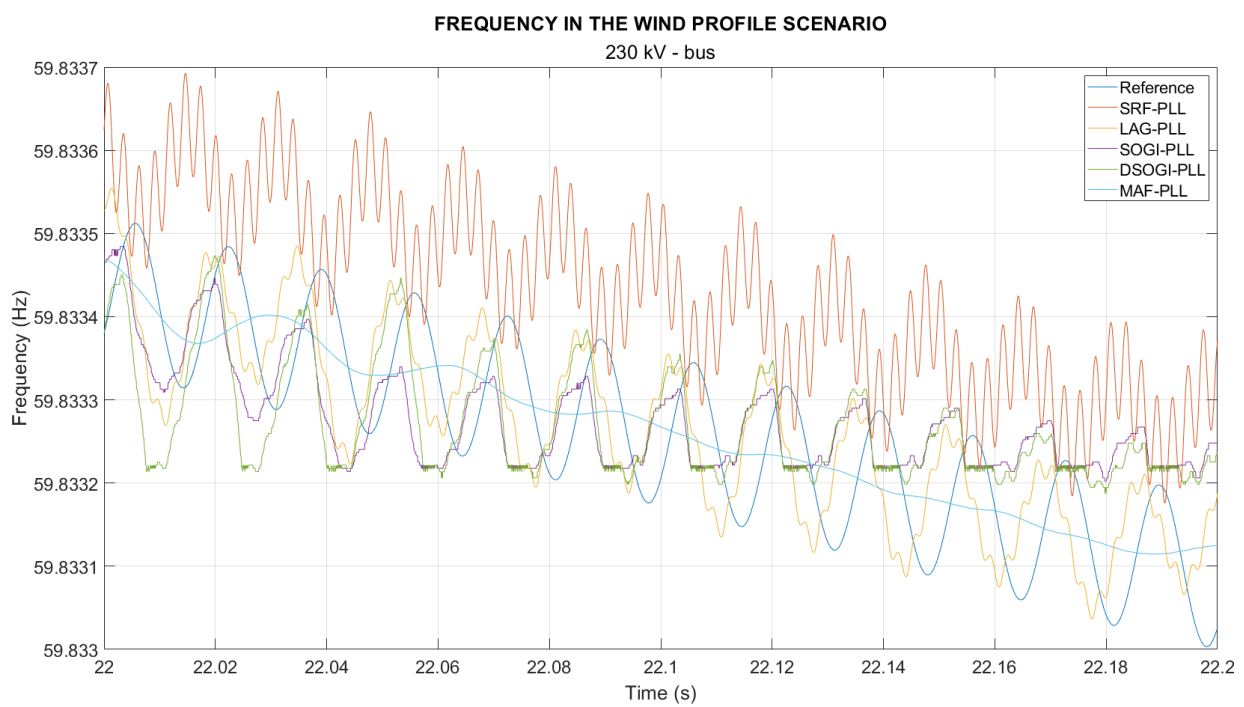
To appreciate the differences, Figure 15b shows a zoomed-in image of the interval from seconds 22 to 22.2. Again, the SRF-PLL presents significant measurement errors. Other PLLs present deviations from the reference, but they are relatively close. In this case, MAF-PLL and SOGI-PLL are closer to the reference during the different oscillations presented. However, the MAF-PLL cannot track the reference oscillations.

Finally, Figure 16 displays frequency measurements with the PLLs located at the low voltage level, 575 V WinGen bus. Figure 16a presents the system frequency measured with the PLLs from seconds 15 to 35, showing that all PLLs obtain a frequency measurement similar to the reference. However, compared to the measurements performed at the higher voltage levels, these measurements show representative and observable differences from the reference values. For a closer look, Figure 16b shows a zoomed-in image of the interval from seconds 22 to 22.2. The magnitude of the errors of SRF-PLL and LAG-PLL increase greatly.

Regarding the metrics of the measurement errors, as defined in Section 2.5, Table 2 shows the relative mean absolute error (MAE%) in quasi-steady-state operation for the PLLs located at the different system buses. The results show that the MAE% is low when measuring the frequency with the PLLs in the 230 kV buses, and those values increase at lower voltage levels. SOGI-PLL presents lower MAE than the other PLLs measuring in the 25 kV and 575 V buses. MAF-PLL is the best method to measure the frequency in the 230 kV buses. The MAE values for the SRF-PLL and LAG-PLL are similar for all cases except for the 575 V bus, where a slight difference can be observed.

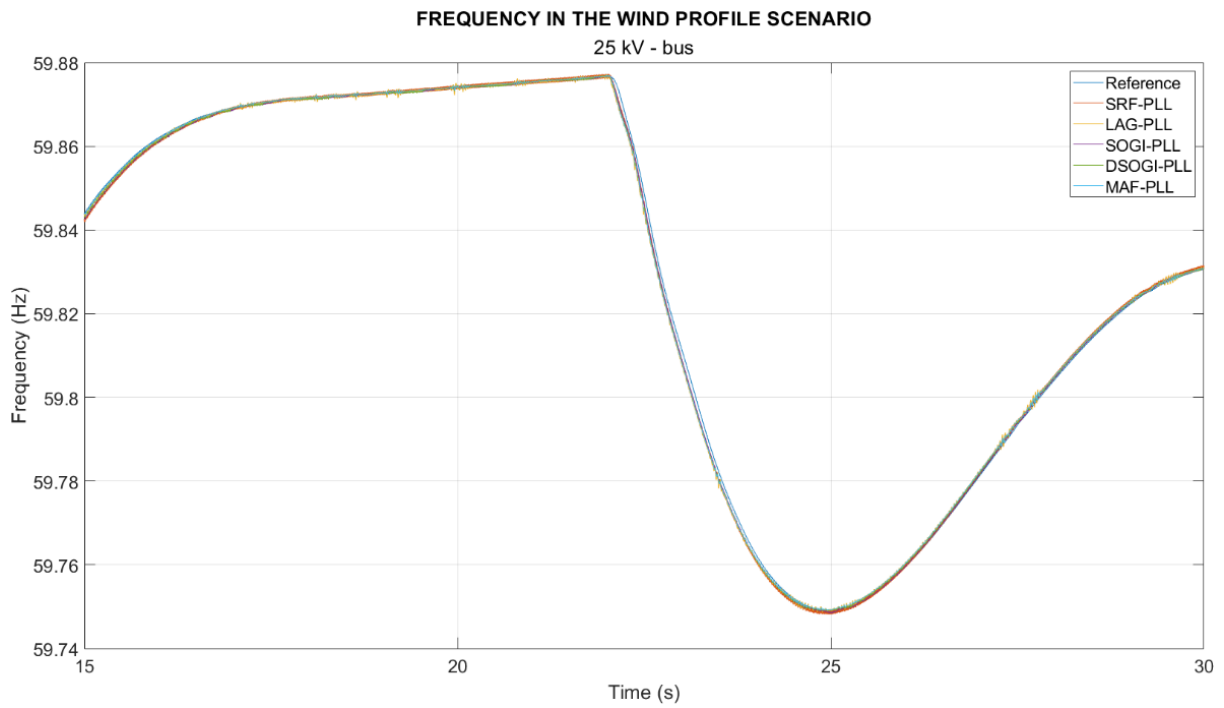


(a)

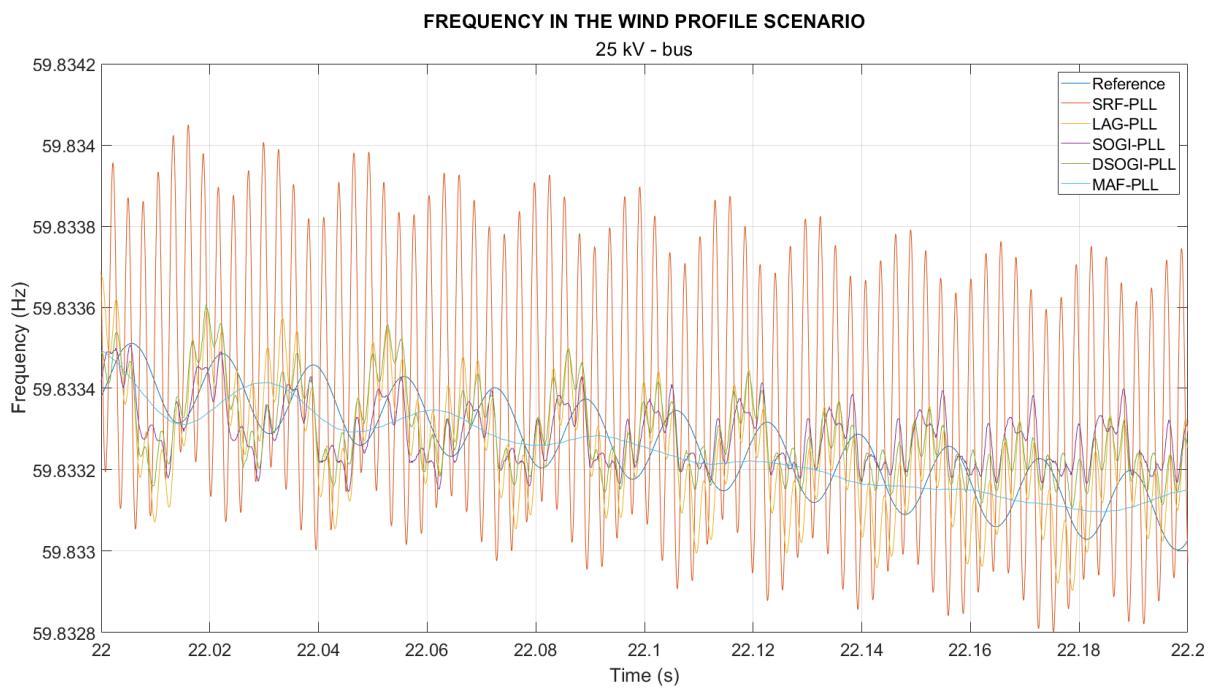


(b)

**Figure 14.** Frequency measurement with the PLLs located at the 230 kV bus: (a) PLLs measuring from seconds 15 to 35, and (b) detail of the measurements from seconds 22 to 22.2.



(a)



(b)

**Figure 15.** Frequency measurement with the PLLs located at the 25 kV WinGen bus: (a) PLLs measuring from seconds 15 to 35, and (b) detail of the measurements from seconds 22 to 22.2.

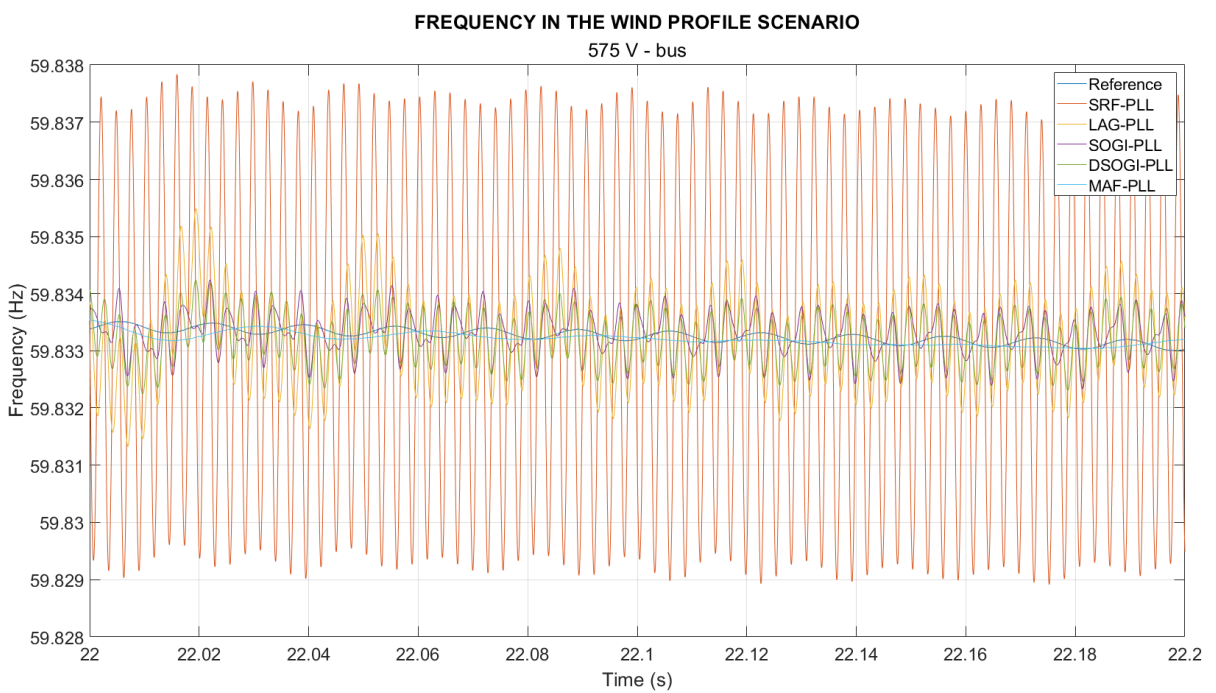
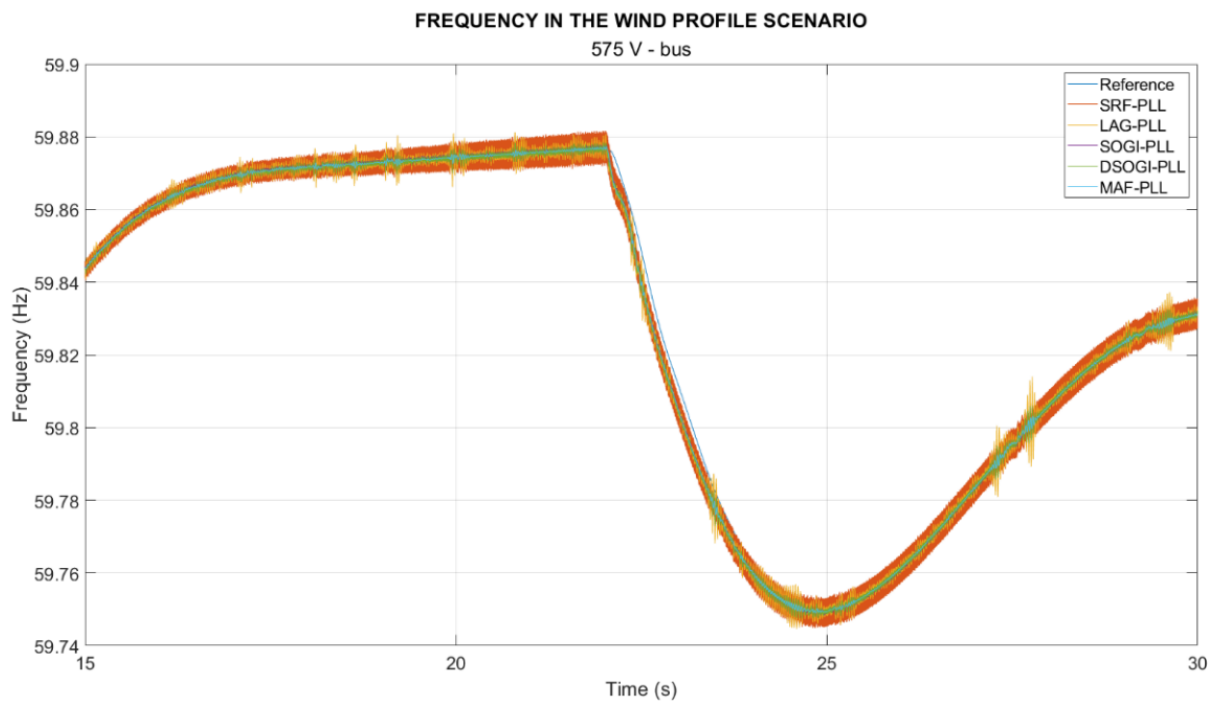


**Figure 16.** Frequency measurement with the PLLs located at the 575 V bus: (a) PLLs measuring from seconds 15 to 35, and (b) detail of the measurements from seconds 22 to 22.2.

**Table 2.** Relative mean absolute error for the PLLs located at the different buses in the constant wind speed scenario.

PLL	MAE% (Constant Wind Speed Scenario)				
	230 kV SynGen	230 kV WinGen	230 kV Load	25 kV WinGen	575 V WinGen
SRF-PLL	0.0385%	0.0385%	0.0380%	0.0628%	0.1728%
LAG-PLL	0.0377%	0.0377%	0.0371%	0.0667%	0.1437%
SOGI-PLL	0.0361%	0.0361%	0.0360%	0.0447%	0.1064%
DSOGI-PLL	0.0333%	0.0333%	0.0329%	0.0551%	0.1205%
MAF-PLL	0.0317%	0.0317%	0.0316%	0.0566%	0.1191%

Regarding the root-mean-square error (RMSE), all the PLLs give acceptable values for their measurements. In this case, the relative error (RMSE%) is close to 0.001%, which can be considered negligible in steady-state operation, and therefore inconclusive. Table 3 shows the RMSE% values obtained with the different PLLs located at the system buses in a constant wind speed scenario. All PLLs provide similar results, but lower values were obtained for the MAF-PLL at the different buses. In addition, the RMSE values for the SRF-PLL and the LAG-PLL were the same for all buses.

**Table 3.** Relative RMSE values for the PLLs located at the different buses in the constant wind speed scenario.

PLL	RMSE% (Constant Wind Speed Scenario)				
	230 kV SynGen	230 kV WinGen	230 kV Load	25 kV WinGen	575 V WinGen
SRF-PLL	0.000172%	0.000172%	0.000179%	0.000256%	0.000396%
LAG-PLL	0.000172%	0.000172%	0.000179%	0.000256%	0.000396%
SOGI-PLL	0.000542%	0.000542%	0.000548%	0.000369%	0.000403%
DSOGI-PLL	0.000333%	0.000333%	0.000326%	0.000301%	0.000319%
MAF-PLL	0.000020%	0.000020%	0.000020%	0.000102%	0.000267%

The AEFD also provides essential information for determining the performance of the PLLs. The cumulative relative AEFD (CAEFD%) was computed in all cases in the manner defined in Equation (15), and the results are compiled in Table 4. The results show that the SRF-PLL is the most affected at all voltage buses. The SRF-PLL, LAG-PLL, SOGI-PLL, and DSOGI-PLL produce a significant deviation in the 25 kV and 575 V buses; however, the MAF-PLL behaves better at these voltage levels compared to the other PLLs. In addition, MAF-PLL has a similar percentage at the 230 kV and 575 V buses, except for the 25 kV bus, where the percentage increases. DSOGI-PLL presents the best behavior of the PLLs in this indicator.

**Table 4.** Cumulative relative AEFD values for the PLLs located at the different buses in the constant wind speed scenario.

PLL	CAEFD% (Constant Wind Speed Scenario)				
	230 kV SynGen	230 kV WinGen	230 kV Load	25 kV WinGen	575 V WinGen
SRF-PLL	190.54%	190.54%	249.63%	1770.19%	9277.65%
LAG-PLL	25.50%	25.50%	12.97%	341.27%	1981.73%
SOGI-PLL	13.65%	13.65%	15.76%	115.26%	716.09%
DSOGI-PLL	9.38%	9.38%	3.90%	168.94%	1152.07%
MAF-PLL	43.10%	43.10%	42.91%	18.24%	48.21%

Similar results are obtained by using the cumulative relative RMSEFD, as shown in Table 5.

**Table 5.** Cumulative RMSEFD values for the PLLs located at the different buses in the constant wind speed scenario.

PLL	CRMSEFD% (Constant Wind Speed Scenario)				
	230 kV SynGen	230 kV WinGen	230 kV Load	25 kV WinGen	575 V WinGen
SRF-PLL	174.12%	174.12%	226.00%	1621.03%	8536.99%
LAG-PLL	30.63%	30.63%	18.89%	327.67%	1847.97%
SOGI-PLL	73.38%	73.38%	71.07%	193.20%	797.12%
DSOGI-PLL	93.39%	93.39%	88.71%	227.48%	1085.21%
MAF-PLL	28.52%	28.52%	28.35%	1.48%	79.38%

### 3.2. Scenario 2: Variable Wind Speed

Figure 17 displays the frequency measurement with the PLLs located at the 230 kV WinGen bus in the variable wind speed scenario. Figure 17a presents the frequency in a wide period from seconds 100 to 450. All PLLs present frequency measurements similar to the reference. However, as in previous figures, there are slight differences in the PLLs that are not easily perceived because of the scale.

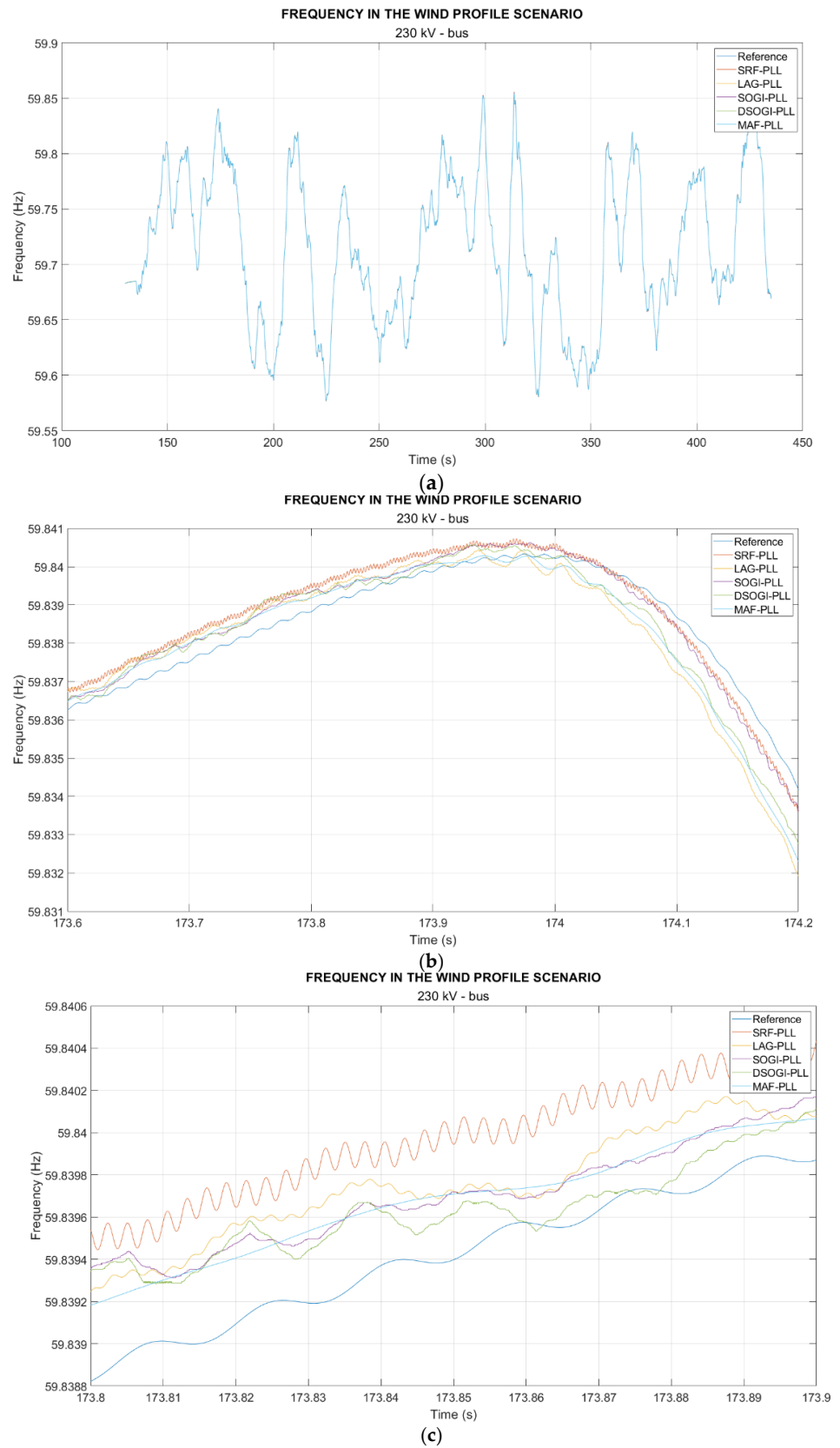
To better appreciate the differences, Figure 17b,c show some details with different zoom levels. This shows that all PLLs introduce some differences from the reference, but most are close to representing the same behavior. In addition, the MAF averages the frequency signal more linearly than the other PLLs. The SRF-PLL shows the worst performance in the 230 kV network.

Figure 18 displays the frequency measurement with the PLLs located at the 25 kV WinGen bus in the variable wind speed scenario. Figure 18a presents the frequency in a wide period from 100 to 450 s. This result reveals that all PLLs present frequency measurements similar to the reference, and no difference is appreciable in this range. To better appreciate the differences, Figure 18b,c show some details with different zoom levels. Both figures show that all PLLs show significant differences regarding the reference, but some represent the form of the reference signal better. In addition, they are not in phase with the reference, and MAF-PLL has fewer variations in the frequency measurement. The noise of the frequency signal generated by the SRF-PLL and LAG-PLL increases slightly.

Figure 18 shows analogous frequency measurements, but with the PLLs located at the 25 kV WinGen bus. Figure 18a presents the system frequency measured with the PLLs from seconds 100 to 450; Figure 18b, from seconds 173.8 to 174.1; and Figure 18c, from 173.8 to 173.9. The last figures show that all of the PLLs show significant differences from the reference, but some represent the form of the reference signal. In addition, they are not in phase with the reference, and MAF-PLL has fewer variations. SRF-PLL and LAG-PLL behave the worst.

Finally, Figure 19 displays frequency measurements with the PLLs located at the low voltage level, the 575 V WinGen bus, with three different zoom levels. Compared to the measurements performed at the higher voltage levels, these measurements show greater differences from the reference values. SFT-PLL introduces a wider variation with respect to the frequency measurement. The frequency measurements performed with LAG-PLL, SOGI-PLL, DSOGI-PLL, and MAF-PLL are close to each other.

The metrics of measurement errors, as defined in Section 2.5, are compiled in Tables 6–9 for the variable wind speed scenario in the interval from second 130 to second 430. Table 6 shows the relative mean absolute error (MAE%). The results show that LAG-PLL presents the highest measurement error in the 230 kV network, followed by DSOGI-PLL. In addition, MAF-PLL produces a lower error. SOGI-PLL, DSOGIPLL, and MAF-PLL give lower measurement errors in the 25 kV and 575 V networks. Furthermore, SOGI-PLL gives the lowest error values in the 25 kV WinGen bus.



**Figure 17.** Frequency measurement with the PLLs located at the 230 kV WinGen bus in the variable wind speed scenario. The measurements are shown with different zoom levels: (a) from seconds 100 to 450, (b) from seconds 173.6 to 174.2, and (c) from seconds 173.8 to 173.9.

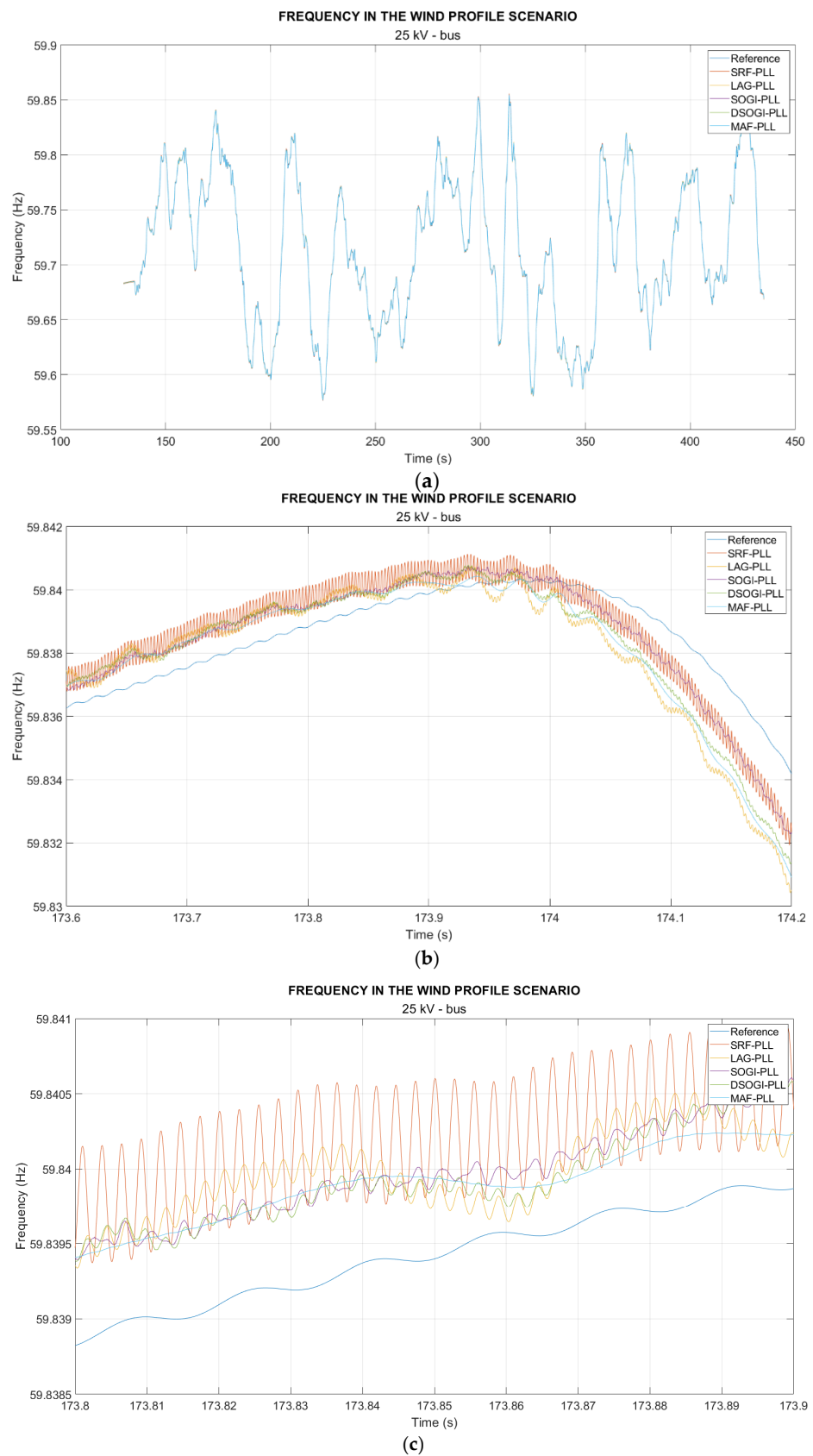


**Figure 18.** Frequency measurement with the PLLs located at the 25 kV WinGen bus in the variable wind speed scenario. The measurements are shown with different zoom levels: (a) from seconds 100 to 450, (b) from seconds 173.6 to 174.2, and (c) from seconds 173.8 to 173.9.

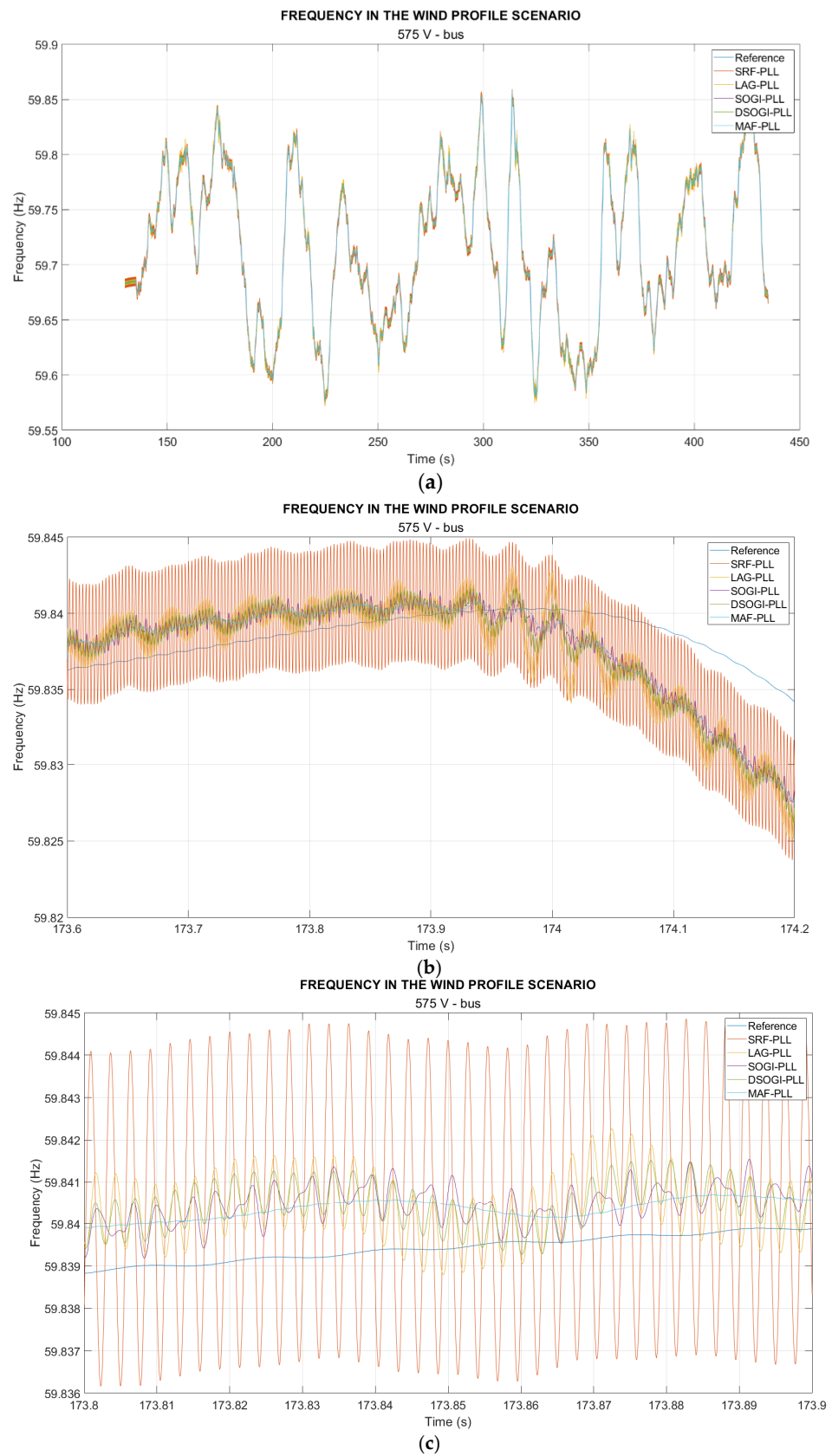


**Figure 19.** Frequency measurement with the PLLs located at the 575 kV WinGen bus in the variable wind speed scenario. The measurements are shown with different zoom levels: (a) from seconds 100 to 450, (b) from seconds 173.6 to 174.2, and (c) from seconds 173.8 to 173.9.

**Table 6.** Relative mean absolute error for the PLLs located at different buses in the variable wind speed scenario.

PLL	MAE% (Variable Wind Speed Scenario)				
	230 kV SynGen	230 kV WinGen	230 kV Load	25 kV WinGen	575 V WinGen
SRF-PLL	0.0221%	0.0221%	0.0222%	0.0477%	0.1614%
LAG-PLL	0.0259%	0.0259%	0.0258%	0.0506%	0.1187%
SOGI-PLL	0.0218%	0.0218%	0.0217%	0.0341%	0.0771%
DSOGI-PLL	0.0245%	0.0245%	0.0244%	0.0405%	0.0898%
MAF-PLL	0.0200%	0.0200%	0.0200%	0.0395%	0.0866%

**Table 7.** Relative RMSE values for the PLLs located at different buses in the variable wind speed scenario.

PLL	RMSE% (Variable Wind Speed Scenario)				
	230 kV SynGen	230 kV WinGen	230 kV Load	25 kV WinGen	575 V WinGen
SRF-PLL	0.000025%	0.000025%	0.000025%	0.000032%	0.000064%
LAG-PLL	0.000025%	0.000025%	0.000025%	0.000032%	0.000064%
SOGI-PLL	0.000043%	0.000043%	0.000043%	0.000050%	0.000075%
DSOGI-PLL	0.000043%	0.000043%	0.000043%	0.000050%	0.000064%
MAF-PLL	0.000018%	0.000018%	0.000018%	0.000032%	0.000057%

**Table 8.** Cumulative relative AEFD values for the PLLs located at different buses in the variable wind speed scenario.

PLL	CAEFD% (Variable Wind Speed Scenario)				
	230 kV SynGen	230 kV WinGen	230 kV Load	25 kV WinGen	575 V WinGen
SRF-PLL	658.37%	658.37%	823.96%	4807.51%	24742.68%
LAG-PLL	141.30%	141.30%	165.67%	1040.80%	5488.64%
SOGI-PLL	68.84%	68.84%	73.67%	419.08%	1993.61%
DSOGI-PLL	139.75%	139.75%	145.96%	583.90%	3263.35%
MAF-PLL	12.99%	12.99%	13.50%	86.07%	262.25%

**Table 9.** Cumulative RMSEFD values for the PLLs located at different buses in the variable wind speed scenario.

PLL	CRMSEFD% (Variable Wind Speed Scenario)				
	230 kV SynGen	230 kV WinGen	230 kV Load	25 kV WinGen	575 V WinGen
SRF-PLL	455.37%	455.37%	574.22%	3469.70%	17951.74%
LAG-PLL	103.61%	103.61%	118.63%	757.63%	4003.72%
SOGI-PLL	198.87%	198.87%	203.23%	461.29%	1731.32%
DSOGI-PLL	255.17%	255.17%	259.94%	544.70%	2390.31%
MAF-PLL	13.86%	13.86%	14.29%	83.03%	262.22%

Table 7 shows the RMSE% values obtained with the different PLLs located at the system buses. Although the RMS values were not conclusive in the 25 kV network, the results show that SRF-PLL, LAG-PLL, and MAF-PLL were able to obtain the values closest to the reference (i.e., low errors). However, after analyzing all errors, they were not very sensitive to small disturbances such as wind speed change, but were very sensitive to noise.

Table 8 shows the cumulative relative AEFD (CAEFD). In this case, SRF-PLL presented the highest differences of all PLLs, and the lowest was obtained with MAF-PLL. The errors increase at lower system voltages for all PLLs, and MAF-PLL presents the lowest

values. Therefore, MAF-PLL gives a clear advantage with respect to the AEFD for all of the evaluated cases.

Similar results were obtained when using the cumulative relative RMSEFD, as shown in Table 9.

### 3.3. Summary of Results

After testing the PLLs located at different buses in a power system with generators and considering two scenarios, the following summary was extracted from the results:

- SRF-PLL: It is more sensitive to small frequency changes produced by wind speed variations. Therefore, the method is more suitable for frequency measurements in a constant wind speed scenario than in a variable wind speed scenario. However, it is more sensitive to voltage harmonics, generating more significant noise than other PLLs.
- LAG-PLL: In the constant wind speed scenario, the LAG-PLL behaves better than the SRF-PLL, making it suitable for applications where it is unnecessary to consider the dynamic behavior of the frequency. A filter of the voltage signal before the PI makes it unreliable for dynamic behavior, as demonstrated with the frequency measurement in the variable wind speed scenario.
- SOGI-PLL: Frequency measurements in the lower voltage levels are accurate in the two simulated scenarios. It provides low error and follows the sinusoidal behavior of the reference, showing a better filtering capacity for the voltage signal facing noise. It is sensitive to the changes produced by small wind speed variations. This PLL is used for single-phase systems and can give errors in the case of unbalanced systems.
- DSOGI-PLL: As the three-phase version of the SOGI-PLL, it offers a sensitivity similar to that of the single-phase version. Although the frequency measurement error is increased, this cannot be considered representative, knowing that this type may become more accurate in unbalanced networks. Because of the sensitivity, it generates noise in the frequency measurement, affecting the RMS value of the frequency derivative. However, the single-phase model and the MAF-PLL are the only ones better.
- MAF-PLL: It is a PLL that responds adequately to the constant wind speed scenario. Although it averages the signal and tries to flatten sine waves, it generates the lowest measurement errors in the constant and variable wind speed scenarios at the higher voltage levels. It can filter the signal to make it less sensitive to slight changes in the measurement or an increase in the noise level of the input signal. This latter behavior was also observed at the lower voltage levels in the constant and variable wind speed scenarios.

## 4. Conclusions

No particular PLL implementation can be recommended as the optimal solution for frequency measurement in a low-inertia power system. The best PLL version depends on the particular characteristics of the system and on the voltage level and location of the generator that is going to make use of the measurements. The optimal PLL for a given application should be selected according to a complete frequency measurement analysis.

**Author Contributions:** O.D.G.-B.: Conceptualization, data curation, investigation, methodology, software, validation, visualization, and writing—original draft; S.M.: Conceptualization, formal analysis, funding acquisition, investigation, methodology, project administration, resources, supervision, and writing—review and editing; J.E.C.-B. and E.M.: Formal analysis, writing—review and editing. All authors have read and agreed to the published version of the manuscript.

**Funding:** This research was funded by the Spanish national research agency Agencia Estatal de Investigación, grant number PID2019-108966RB-I00/AEI/10.13039/501100011033.

**Institutional Review Board Statement:** Not applicable.

**Informed Consent Statement:** Not applicable.

**Data Availability Statement:** Not applicable.

**Acknowledgments:** The authors thank to the Escuela Técnica Superior de Ingenieros Industriales, Universidad Politécnica de Madrid. The work of John E. Candelo-Becerra was supported by Universidad Nacional de Colombia, Sede Medellín.

**Conflicts of Interest:** The authors declare no conflict of interest.

## References

1. Hernández-Callejo, L.; Gallardo-Saavedra, S.; Alonso-Gómez, V. A Review of Photovoltaic Systems: Design, Operation and Maintenance. *Sol. Energy* **2019**, *188*, 426–440. [[CrossRef](#)]
2. Tawalbeh, M.; Al-Othman, A.; Kafiah, F.; Abdelsalam, E.; Almomani, F.; Alkasrawi, M. Environmental Impacts of Solar Photovoltaic Systems: A Critical Review of Recent Progress and Future Outlook. *Sci. Total Environ.* **2021**, *759*, 143528. [[CrossRef](#)] [[PubMed](#)]
3. Peng, Q.; Jiang, Q.; Yang, Y.; Liu, T.; Wang, H.; Blaabjerg, F. On the Stability of Power Electronics-Dominated Systems: Challenges and Potential Solutions. *IEEE Trans. Ind. Appl.* **2019**, *55*, 7657–7670. [[CrossRef](#)]
4. Guerra, K.; Haro, P.; Gutiérrez, R.E.; Gómez-Barea, A. Facing the High Share of Variable Renewable Energy in the Power System: Flexibility and Stability Requirements. *Appl. Energy* **2022**, *310*, 118561. [[CrossRef](#)]
5. Bloom, A.; Helman, U.; Holttinen, H.; Summers, K.; Bakke, J.; Brinkman, G.; Lopez, A. It's Indisputable: Five Facts About Planning and Operating Modern Power Systems. *IEEE Power Energy Mag.* **2017**, *15*, 22–30. [[CrossRef](#)]
6. Liu, B.; An, M.; Wang, H.; Chen, Y.; Zhang, Z.; Xu, C.; Song, S.; Lv, Z. A Simple Approach to Reject DC Offset for Single-Phase Synchronous Reference Frame PLL in Grid-Tied Converters. *IEEE Access* **2020**, *8*, 112297–112308. [[CrossRef](#)]
7. Li, Y.; Fan, L.; Miao, Z. Wind in Weak Grids: Low-Frequency Oscillations, Subsynchronous Oscillations, and Torsional Interactions. *IEEE Trans. Power Syst.* **2020**, *35*, 109–118. [[CrossRef](#)]
8. Ortega, A.; Milano, F. Comparison of Different PLL Implementations for Frequency Estimation and Control. In Proceedings of the 2018 18th International Conference on Harmonics and Quality of Power (ICHQP), Ljubljana, Slovenia, 13–16 May 2018; pp. 1–6.
9. Karimi-Ghartemani, M.; Iravani, M.R. Robust and Frequency-Adaptive Measurement of Peak Value. *IEEE Trans. Power Deliv.* **2004**, *19*, 481–489. [[CrossRef](#)]
10. Liu, C.; Jiang, J.; Jiang, J.; Zhou, Z. Enhanced Grid-Connected Phase-Locked Loop Based on a Moving Average Filter. *IEEE Access* **2020**, *8*, 5308–5315. [[CrossRef](#)]
11. Golestan, S.; Guerrero, J.M.; Vasquez, J.C.; Abusorrah, A.M.; Al-Turki, Y. Standard SOGI-FLL and Its Close Variants: Precise Modeling in LTP Framework and Determining Stability Region/Robustness Metrics. *IEEE Trans. Power Electron.* **2021**, *36*, 409–422. [[CrossRef](#)]
12. Zhang, C.; Foyen, S.; Suul, J.A.; Molinas, M. Modeling and Analysis of SOGI-PLL/FLL-Based Synchronization Units: Stability Impacts of Different Frequency-Feedback Paths. *IEEE Trans. Energy Convers.* **2021**, *36*, 2047–2058. [[CrossRef](#)]
13. Ranjan, A.; Kewat, S.; Singh, B. DSOGI-PLL With In-Loop Filter Based Solar Grid Interfaced System for Alleviating Power Quality Problems. *IEEE Trans. Ind. Appl.* **2021**, *57*, 730–740. [[CrossRef](#)]
14. Nicastrì, A.; Nagliero, A. Comparison and Evaluation of the PLL Techniques for the Design of the Grid-Connected Inverter Systems. In Proceedings of the 2010 IEEE International Symposium on Industrial Electronics, Bari, Italy, 4–7 July 2010; pp. 3865–3870.
15. Silva, S.M.; Lopes, B.M.; Cardoso Filho, B.J.; Campana, R.P.; Boaventura, W.C. Performance Evaluation of PLL Algorithms for Single-Phase Grid-Connected Systems. In Proceedings of the Conference Record of the 2004 IEEE Industry Applications Conference, 2004, 39th IAS Annual Meeting, Seattle, WA, USA, 3–7 October 2004; Volume 4, pp. 2259–2263.
16. Darambazar, G.; Moukadem, A.; Colicchio, B.; Wira, P. A Comparison of PLL for Online Frequency Tracking in Power Grids. In Proceedings of the 2021 IEEE 30th International Symposium on Industrial Electronics (ISIE), Kyoto, Japan, 20–23 June 2021; pp. 1–6.
17. Setiawan, I.; Facta, M.; Priyadi, A.; Purnomo, M.H. Comparison of Three Popular PLL Schemes under Balanced and Unbalanced Grid Voltage Conditions. In Proceedings of the 2016 8th International Conference on Information Technology and Electrical Engineering (ICITEE), Yogyakarta, Indonesia, 5–6 October 2016; pp. 1–6.
18. Royan; Andromeda, T.; Facta, M.; Hermawan; Setiawan, I. Comparison of SOGI-FLL with SOGI-PLL for Single-Phase Grid-Connected Inverters. In Proceedings of the 4th International Conference on Energy, Environment, Epidemiology and Information System (ICENIS 2019), Semarang, Indonesia, 7–8 August 2019.
19. Rueda-Escobedo, J.G.; Tang, S.; Schiffer, J. A Performance Comparison of PLL Implementations in Low-Inertia Power Systems Using an Observer-Based Framework. *IFAC-PapersOnLine* **2020**, *53*, 12244–12250. [[CrossRef](#)]
20. Jamaludin, N.F.; Saidina Omar, A.M.; Isa, S.S.M.; Ahmad, N.D.; Ramli, S.S. Comparison Techniques Using Phase—Loop Locked (PLL) and Synchronous References Frame (SRF) Controller to Mitigate Voltage Flicker. *J. Phys. Conf. Ser.* **2019**, *1349*, 012124. [[CrossRef](#)]
21. Prakash, S.; Singh, J.K.; Behera, R.K.; Mondal, A. Comprehensive Analysis of SOGI-PLL Based Algorithms for Single-Phase System. In Proceedings of the 2019 National Power Electronics Conference (NPEC), Tiruchirappalli, India, 13–15 December 2019; pp. 1–6.

22. Ullah, I.; Ashraf, M. Comparison of Synchronization Techniques Under Distorted Grid Conditions. *IEEE Access* **2019**, *7*, 101345–101354. [[CrossRef](#)]
23. Singh, U.K.; Basak, A. Performance Study of Different PLL Schemes Under Unbalanced Grid Voltage. In Proceedings of the 2019 IEEE Region 10 Symposium (TENSYP), Kolkata, India, 7–9 June 2019; pp. 66–71.
24. Santos Filho, R.M.; Seixas, P.F.; Cortizo, P.C.; Torres, L.A.B.; Souza, A.F. Comparison of Three Single-Phase PLL Algorithms for UPS Applications. *IEEE Trans. Ind. Electron.* **2008**, *55*, 2923–2932. [[CrossRef](#)]
25. Bifaretti, S.; Zanchetta, P.; Lavopa, E. Comparison of Two Three-Phase PLL Systems for More Electric Aircraft Converters. *IEEE Trans. Power Electron.* **2014**, *29*, 6810–6820. [[CrossRef](#)]
26. Godave, A.; Choudhari, P.; Jadhav, A. Comparison and Simulation of Analog and Digital Phase Locked Loop. In Proceedings of the 2018 9th International Conference on Computing, Communication and Networking Technologies (ICCCNT), Bengaluru, India, 10–12 July 2018; pp. 1–4.
27. Aguilera, R.P.; Acuna, P.; Konstantinou, G.; Vazquez, S.; Leon, J.I. Basic Control Principles in Power Electronics. In *Control of Power Electronic Converters and Systems*; Elsevier: Amsterdam, The Netherlands, 2018; pp. 31–68.
28. Zhou, D.; Song, Y.; Blaabjerg, F. Modeling and Control of Three-Phase AC/DC Converter Including Phase-Locked Loop. In *Control of Power Electronic Converters and Systems*; Elsevier: Amsterdam, The Netherlands, 2018; pp. 117–151.
29. Ortega, A.; Milano, F. Impact of Frequency Estimation for VSC-Based Devices with Primary Frequency Control. In Proceedings of the 2017 IEEE PES Innovative Smart Grid Technologies Conference Europe (ISGT-Europe), Turin, Italy, 26–29 September 2017; pp. 1–6.
30. Yuan, X.; Merk, W.; Stemmler, H.; Allmeling, J. Stationary-Frame Generalized Integrators for Current Control of Active Power Filters with Zero Steady-State Error for Current Harmonics of Concern under Unbalanced and Distorted Operating Conditions. *IEEE Trans. Ind. Appl.* **2002**, *38*, 523–532. [[CrossRef](#)]
31. Rodriguez, P.; Luna, A.; Candela, I.; Mujal, R.; Teodorescu, R.; Blaabjerg, F. Multiresonant Frequency-Locked Loop for Grid Synchronization of Power Converters Under Distorted Grid Conditions. *IEEE Trans. Ind. Electron.* **2011**, *58*, 127–138. [[CrossRef](#)]
32. Rodriguez, P.; Teodorescu, R.; Candela, I.; Timbus, A.V.; Liserre, M.; Blaabjerg, F. New Positive-Sequence Voltage Detector for Grid Synchronization of Power Converters under Faulty Grid Conditions. In Proceedings of the 37th IEEE Power Electronics Specialists Conference, Jeju, Korea, 18–22 June 2006; pp. 1–7.
33. Robles, E.; Ceballos, S.; Pou, J.; Zaragoza, J.; Gabiola, I. Grid Synchronization Method Based on a Quasi-Ideal Low-Pass Filter Stage and a Phase-Locked Loop. In Proceedings of the 2008 IEEE Power Electronics Specialists Conference, Rhodes, Greece, 15–19 June 2008; pp. 4056–4061.
34. Report, I. Dynamic Models for Steam and Hydro Turbines in Power System Studies. *IEEE Trans. Power Appar. Syst.* **1973**, *PAS-92*, 1904–1915. [[CrossRef](#)]
35. IEEE Subsynchronous Resonance Working Group of the Dynamic System Performance Subcommittee and Power System Engineering Committee. Second Benchmark Model for Computer Simulation of Subsynchronous Resonance. *IEEE Trans. Power Appar. Syst.* **1985**, *PAS-104*, 1057–1066. [[CrossRef](#)]
36. Kundur, P. *Power System Stability and Control*, 1st ed.; McGraw-Hill, Inc.: Palo Alto, CA, USA, 1994; ISBN 007035958X.
37. Gagnon, R.; Turmel, G.; Larose, C.; Brochu, J.; Sybille, G.; Fecteau, M. Large-Scale Real-Time Simulation of Wind Power Plants into Hydro-Quebec Power System. In Proceedings of the 9th International Workshop on Large-Scale Integration of Wind Power into Power Systems as well as on Transmission Networks for Offshore Wind Power Plants, Québec, QC, Canada, 18–19 October 2010; Betancourt, U., Ackermann, T., Eds.; energynautics GmbH: Québec, QC, Canada, 2010; pp. 73–80.
38. CIGRE Working Group 02 (Study Committee 33). *Guidelines for Representation of Network Elements When Calculating Transients*; Cigré: Paris, France, 1990.
39. IEC 60076-1:2011; Power Transformers—Part 1: General. International Electrotechnical Commission: Geneva, Switzerland, 2011.
40. Hansen, K.S.; Vasiljevic, N.; Sørensen, S.A. *Wind Resource, SCADA Data and Time Series of Wind and Turbine Loads from Tjareborg, DK*; Dataset; Technical University of Denmark: Kongens Lyngby, Denmark, 2021. [[CrossRef](#)]
41. Willmott, C.J.; Matsuura, K. Advantages of the Mean Absolute Error (MAE) over the Root Mean Square Error (RMSE) in Assessing Average Model Performance. *Clim. Res.* **2005**, *30*, 79–82. [[CrossRef](#)]